Elastomer Surfaces with Directionally Dependent Adhesion Strength and Their Use in Transfer Printing with Continuous Roll-to-Roll Applications

*Sang Yoon Yang, Andrew Carlson, Huanyu Cheng, Qingmin Yu, Numair Ahmed, Jian Wu, Seok Kim, Metin Sitti, Placid M. Ferreira, Yonggang Huang, and John A. Rogers**

Transfer printing has proven to be a versatile tool for deterministic assembly of two and three dimensional structures of diverse materials, with feature sizes from the cm to the nm range.[1–10] The process exploits soft, elastomeric stamps in two steps: i) retrieval of selected collections of objects from a substrate where they are formed, and ii) delivery to a substrate of interest, in a single-step, parallel fashion. The ability to modulate the degree of adhesion between the objects and the surface of the stamp is critically important for effective operation. Various schemes, some inspired by biology and others by basic aspects of adhesion between viscoelastic materials, have been demonstrated.[11,12] Here we introduce geometric designs in relief features on stamps that provide adhesion switching by control of the direction of retraction. In particular, angled posts on the stamp surface lead to changes in the propensity for crack formation, and therefore adhesion strength, depending on the direction of retraction. Such directional microstructures are also observed in geckos and insect foot-hairs.[13–18] Angled micro/nanofibers with saucer-shaped tip endings enable high friction and adhesion strength in the gripping direction by combined vertical and lateral loading; they have significantly less strength in the release direction for power efficient and fast detachment. Such directional adhesives can also be mimicked synthetically in polymer micro/nanofiber structures.[19–21] These systems have been studied for applications in wall-climbing robots[22] and reusable adhesives[19,21], but they have not been explored in geometries suitable for transfer printing. This paper shows that related physics in angled posts of relief on bulk elastomers not only allow high contrast modulation of adhesion in a manner suitable for printing in the usual, batch mode, but that when implemented with cylindrical stamps it provides a pathway to continuous, roll-to-roll operation. We describe methods for fabricating these types of stamps, the key aspects that govern the physics of adhesion in combined experimental and theoretical work, and several representative printing demonstrations.

Figure 1a shows a scanning electron microscopy (SEM) image of a stamp made of poly(dimethylsiloxane) (PDMS) with an array of angled posts, molded on its surface. Critical design aspects include well-defined structures (Figure 1b) with sharp perimeter edges to facilitate controlled crack initiation and propagation for efficient printing, as described subsequently. To achieve this structure, a combination of anti-reflection (thickness ~160 nm) and adhesion promoting (thickness ~ 13 nm) layers were applied to a silicon substrate, followed by photopatterning of a thick layer of epoxy through an amplitude photomask in an angled exposure geometry (Figure S1b). Casting and curing a prepolymer of PDMS onto this substrate, and then peeling the resulting material away yielded the desired stamps. For cases reported here, the tilt angle was 17°. We chose an angle of 17° due to its relative ease in fabrication, its ability to maintain useful levels of maximum adhesion while, at the same time, to provide good contrast in adhesion.

Prof. J. A. Rogers
Department of Materials Science and Engineering
Chemistry, Mechanical Science and Engineering
Electrical and Computer Engineering
Beckman Institute for Advanced Science and Technology
and Frederick Seitz Materials Research Laboratory
University of Illinois at Urbana-Champaign
Urbana, IL 61801, USA
E-mail: jrogers@illinois.edu

Dr. S. Y. Yang, A. Carlson
Department of Materials Science and Engineering
University of Illinois at Urbana-Champaign
Urbana, IL 61801, USA

H. Cheng, Prof. Y. Huang
Department of Mechanical Engineering
Department of Civil and Environmental Engineering
Northwestern University
Evanston, IL 60208, USA

DOI: 10.1002/adma.201104975

Prof. Q. Yu
School of Mechanics, Civil Engineering and Architecture
Northwestern Polytechnical University
Xi'an 710072, China
Department of Mechanical Engineering
Department of Civil and Environmental Engineering
Northwestern University
Evanston, IL 60208, USA

N. Ahmed, Prof. S. Kim, Prof. P. M. Ferreira
Department of Mechanical Science and Engineering
University of Illinois at Urbana-Champaign
Urbana, IL 61801, USA

Prof. J. Wu
Department of Engineering Mechanics
Tsinghua University
Beijing 100084, China

Prof. M. Sitti
Department of Mechanical Engineering
Carnegie Mellon University
Pittsburgh, PA 15213, USA

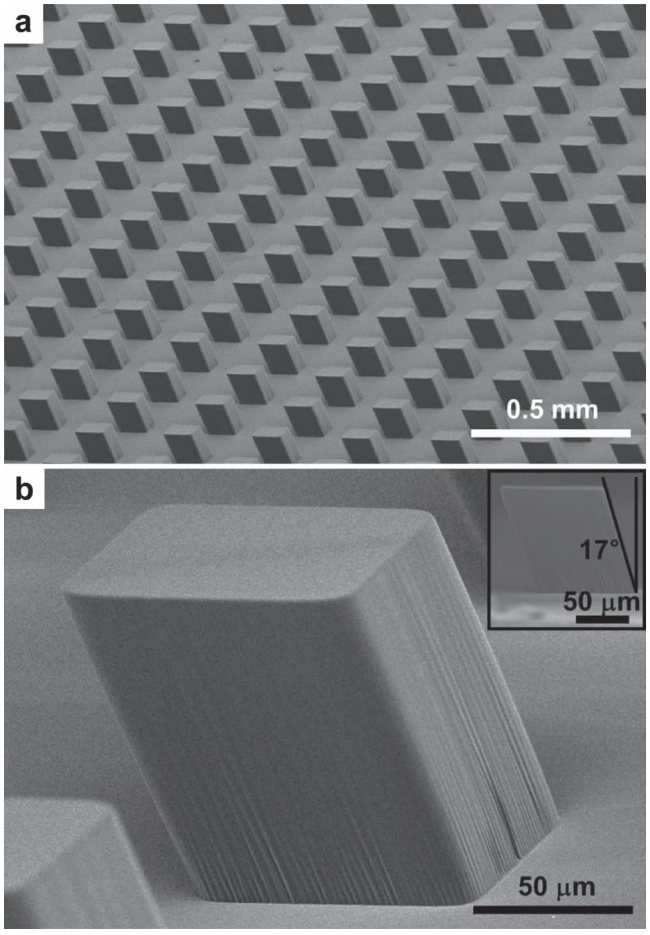

Figure 1. (a) SEM image of an elastomeric stamp with an array of angled posts on its surface. The lateral dimensions of an individual post are 100 μm × 100 μm with a vertical heights of 100 μm. The rectangular stamp (8.2 mm × 19.3 mm) includes 1820 angled posts. (b) SEM image of an single, angled post. The angle of inclination is ~17° relative to the surface normal.

Figure 2a illustrates the principle behind the dependence of adhesion strength on the direction of retraction. An angled post in contact with a flat substrate has natively asymmetric contact angles (θ_a and θ_b, inset, Figure 2a), in contrast to the symmetric, 90° angles of vertical post designs explored previously (inset of Figure 2b). The two contact angles satisfy $\theta_a + \theta_b = 180°$, due to the parallel configuration of the two sides of the post. Since θ_a is smaller than θ_b, a crack at the post/substrate interface propagates preferentially from the corner at θ_a, corresponding to a characteristic pull-off force (F_2) when a vertical force is applied to the stamp. Pulling the post with a component of applied force that lies in a direction opposite to that of the orientation of the angle accelerates crack propagation from the corner θ_a, resulting in a reduced pull-off force ($F_3 < F_2$). By contrast, crack propagation is frustrated when the pulling direction involves force aligned along the other orientation, leading to increased pull-off force ($F_1 > F_2$). Thus, three different regimes of pull-off force ($F_1 > F_2 > F_3$) can be achieved, simply by controlling the direction of the applied separation loads. In transfer printing, these conditions correspond to different magnitudes of force applied to material structures, and can be exploited in this process by choosing the retraction direction during retrieval and delivery to lie along and against the angled axis, respectively.

To quantify this adhesion physics, we evaluated the normal direction pull-off forces under various loading conditions. An adhesion test setup described elsewhere,[9,23] was used to bring a single angled post into intimate contact with the clean surface of a silicon wafer, and then to subject it to increasing displacements, u, in the $\pm x$ directions (corresponding to a well-defined shear strain), with a final retraction in the z direction, away from the substrate surface. Pull-off forces, F, for each displacement were determined by recording force-distance curves with a precision load cell.[23] This combination of lateral displacements and vertical pulling simulates directional retraction along or against the orientation of angle of the angled post. Pull-off forces for a vertical post stamp under the same displacement procedures were also measured for comparison. Figure S2 provides schematic illustrations for each test.

Figure 2a and b show the normalized pull-off force, $P = F/(EL^2)$ where E and L are the Young's modulus and width of the PDMS posts, respectively, as functions of shear strain γ for the angled and the vertical post cases, respectively. For a vertical post, the peak value of P (P_{max}) appeared at $\gamma = 0$, with a symmetric distribution around this condition (Figure 2b). By contrast, for an angled post, the shear strain corresponding to P_{max} for this case was shifted to a positive value of γ (3.6% and 4.8% from experimental data and theoretical result, respectively), with an overall asymmetric distribution (Figure 2a). These results indicate that the adhesion behavior in an angled stamp is dependent on the displacement direction, with large values of P obtained by applying optimum γ along directions that inhibit crack propagation (+x direction in Figure 2a). Comparatively small values of P occur for shear strains along the direction that accelerates crack propagation (–x direction in Figure 2a), or large values in either direction.

These behaviors can be analyzed by a mechanics model of interfacial delamination. A post of height h is subject to a vertical pull-off force F and a shear displacement u imposed at the bottom of the post via the post/substrate interface (Figure 2a). The asymmetric pull-off force F results in a bending moment $Fh\cot\theta_a$ on the post. The shear displacement u gives a shear strain $\gamma = u/(h + 0.421L)$ in the post,[23] which in turn results in a bending moment $\mu\gamma hL^2$ due to shear, where the shear modulus of the post is $\mu = E/3$, E is the Young's modulus, and the post is treated as incompressible. The net bending moment on the post is $M = Fh\cot\theta_a + \mu\gamma hL^2$. Either of two infinitesimal edge cracks at the different corners of the post/substrate contact interface, may propagate and lead to delamination. The corresponding stress intensity factors are obtained analytically in terms of F and the bending moment M.[24] For the limit of vanishing crack length, the crack tip energy release rates, normalized by EL, are given analytically in terms of F and M, or equivalently, F and the shear strain γ

$$\frac{G_{1,2}}{EL} = 0.113\left(\frac{F}{EL^2}\right)^2 + 0.0522\frac{h^2}{L^2}\left(3\frac{F}{EL^2}\cot\theta_a - \gamma\right)^2 \pm 0.0928\frac{h}{L}\frac{F}{EL^2}\left(3\frac{F}{EL^2}\cot\theta_a - \gamma\right), \quad (1)$$

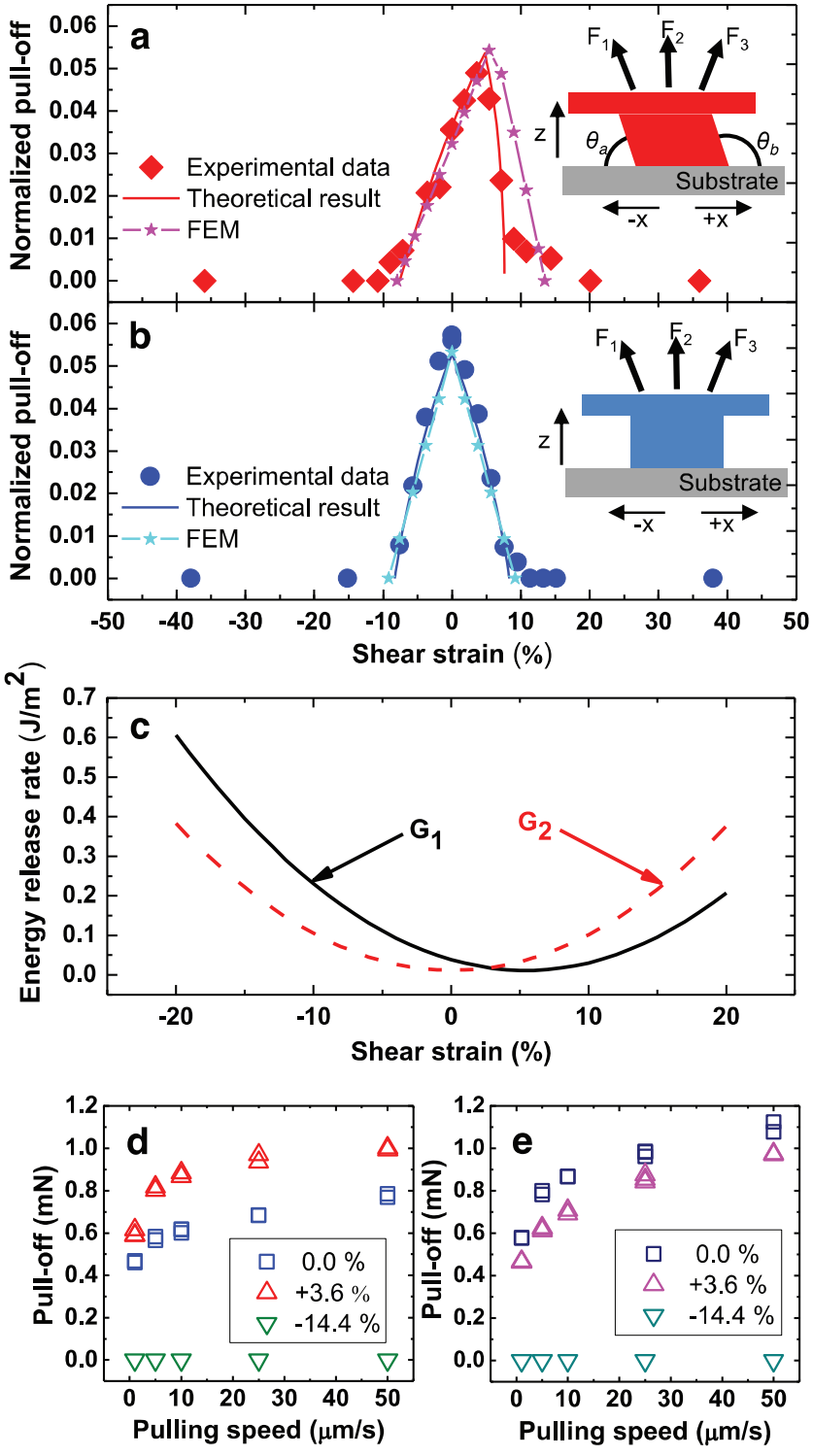

Figure 2. Normalized pull-off force for (a) an angled and (b) a vertical post as a function of shear strain. Symbols (diamonds, circles) and lines represent experimental and theoretical results, respectively. Lines with star symbols show results from finite element method (FEM). The pulling speed in both cases was 10 μm/s. Insets in (a) and (b) show the geometries for an angled and a vertical post, respectively. Arrows over the posts indicate the retraction directions and F_1, F_2, and F_3 are the corresponding forces required for the delamination of post from a substrate. (c) Crack tip energy release rates (G_1, G_2) at the left and right corners of the post/silicon interface as a function of shear strain. Measured pull-off forces for (d) an angled and (e) a vertical post as a function of pulling speed for three different shear strains.

where the subscripts 1 and 2 denote the crack tips at the left and right corners of the post/substrate interface in Figure 2a, respectively, and where the large elastic match between the post (PDMS) and substrate for an interfacial crack tip has been accounted for.[25] For negative shear ($\gamma < 0$, Figure 2c) or relatively small shear in the positive direction $\gamma \leq 3\frac{F}{EL^2}\cot\theta_a$, the left crack tip has a larger energy release rate than the right one. The opposite holds for when $\gamma > 3\frac{F}{EL^2}\cot\theta_a$. Crack propagation starts once the left or right crack tip energy release rates in Equation (1) reach the interfacial fracture toughness Γ_0. This condition gives analytically the critical pull-off force

$$\frac{F}{EL^2} = f\left(\frac{h}{L}\gamma, \frac{h}{L}\cot\theta_a, \frac{\Gamma_0}{EL}\right), \tag{2}$$

which depends the normalized shear strain $(h/L)\gamma$, contact angle $(h/L)\cot\theta_a$, and interfacial fracture toughness $\Gamma_0/(EL)$. For a vertical post ($\theta_a = 90^o$), the pull-off force is given by

$$\frac{F}{EL^2} = \sqrt{8.86\frac{\Gamma_0}{EL} - 0.293\frac{h^2}{L^2}\gamma^2} - 0.411\frac{h}{L}|\gamma|. \tag{3}$$

Equations (2) and (3) agree well with experimental data as shown in Figure 2a and b for the interfacial toughness $\Gamma_0 = 0.057$ N/m.

The finite element method (FEM), with edge cracks of 0.98 μm, further validates the above analytical model. For a similar system, FEM gives a maximum F that is almost the same (1.1% larger) as the analytical solution. The value of γ at which this value of F is reached is 5.4%, by FEM, and 4.8% by the analytical model.

As shown in Figure 2d and e, F measured using both the angled post and the vertical post also exhibit rate-dependent behaviors consistent with viscoelastic materials.[11,12] For zero and positive shear strain conditions, F exhibited a monotonic increase with retraction speed. In the case of an angled post, the values of F at $\gamma = 0$ were smaller than those at the optimum γ (+3.6%) irrespective of the retraction speed, as predicted above ($F_1 > F_2 > F_3$).

The high adhesion switchability afforded by the angled post design enables efficient transfer printing onto a wide range of substrate types, including challenging cases such as those that present significant features of surface relief. As shown in Figure S3, during this process, the adhesion was controlled by a combination of mechanical deformation

(lateral displacement) and viscoelastic effects (retraction speed). During retrieval, maximum adhesion was achieved with optimized lateral displacement (Figure 2) and high retraction speeds. An object retrieved in this manner was then contacted against a substrate of interest, followed by application of sufficient lateral displacement. Delivery was completed by slowly retracting the stamp while holding an applied lateral displacement for minimized adhesion, to facilitate release. **Figure 3** provides examples of printed platelets of silicon (lateral dimensions of 100 μm × 100 μm, thickness of 3 μm) onto silicon substrates with posts and ridges micromachined on their surfaces. The estimated fractional contact area between the platelets and these substrates ranges from 25% (post, Figure 3a) to 14% (ridge, Figure 3b and c). More challenging structures such as freely suspended cantilevers (Figure 3c) were also possible.

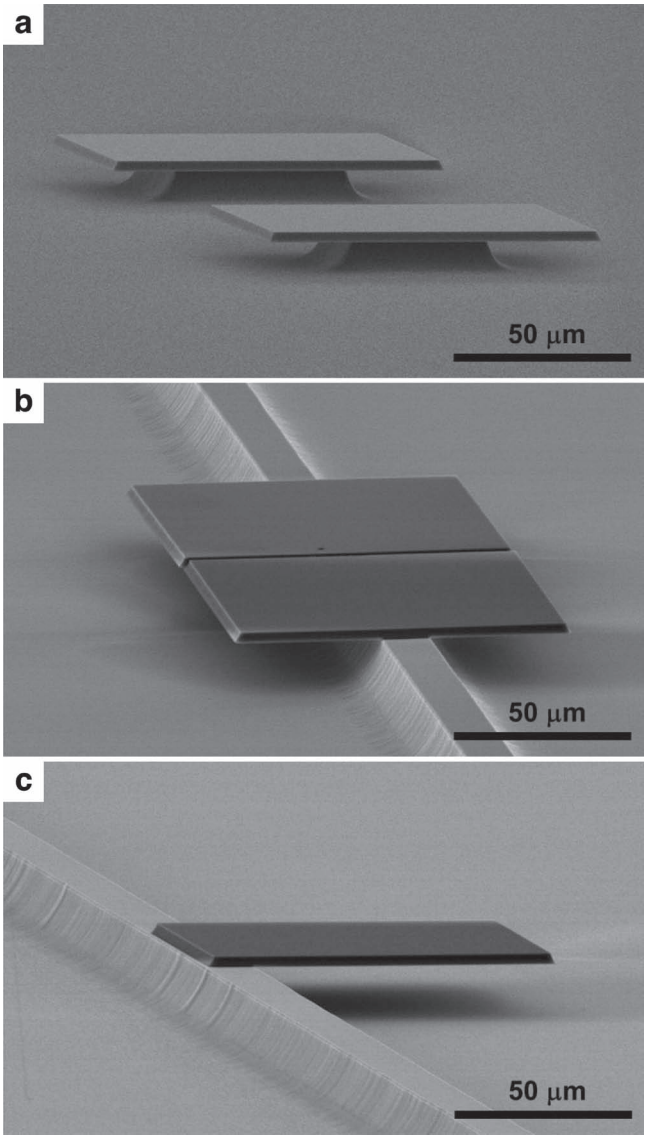

Figure 3. SEM images of printed silicon platelets (lateral dimensions of 100 μm x 100 μm, thicknesses of 3 μm) on micromachined silicon substrates using a single angled post. Platelets printed on posts of silicon (a) with heights of 10 μm and lateral dimensions of 40 μm x 40 μm (front post) and 50 μm x 50 μm (rear post). Printed platelets on the surface of a ridge of silicon (14 μm width) with (b) center and (c) edge alignment of the platelet to the ridge.

Although the performance of the angled post is similar to that of the corresponding vertical case in terms of adhesion switchability under strain (a factor of ~100), the angular dependence of the angled post offers some interesting possibilities. One example is in the realization of roller modes of operation for transfer printing. To demonstrate feasibility, a cylindrical angled post stamp (**Figure 4**a) was fabricated by wrapping a thin sheet of PDMS with angled posts (described in Figure 1) around an aluminum cylinder. The adhesion switchability of such a stamp can be demonstrated, and quantified, by rolling it down an inclined glass plate and comparing the behaviors for the two possible rolling directions. For the case of forward rolling, the angled posts formed a relatively small contact angle to the plate (upper inset, Figure 4b). The opposite (backward) rolling direction involved larger contact angles (lower inset, Figure 4b). In both cases, the stamp reached constant rolling speed (terminal velocity), due to viscoelastic effects. The energy release rate can be calculated from the rate of loss in gravitational potential energy for rolling in this regime.[11] As shown in Figure 4b, the energy release rate for the backward direction is substantially lower than that for the forward, for all rolling speeds, consistent with expectation. FEM can be used to calculate the energy release rate G for these two cases. The length of edge crack along the PDMS/glass interface ranges from zero (for an infinitesimal crack) to the post width (for complete delamination of the interface), and G is then averaged over all crack lengths to represent the average energy release rate during steady-state rolling. Under the same gravitational force, G for forward rolling is larger than that for backward rolling. For a PDMS/glass interface, the interfacial fracture toughness, or critical energy release rate G_c, increases monotonically with the terminal velocity v due to viscoelasticity of PDMS, and can be expressed via a power-law[12]

$$G_c = G_0\left[1 + \left(\frac{v}{v_0}\right)^n\right]. \quad (4)$$

Feng et al.[12] reported the exponent $n = 0.65$ and reference speed $v_0 = 1.55\ \mathrm{cm \cdot s^{-1}}$ in experiments with flat slabs of PDMS; G_0 is the critical energy release rate for a vanishing crack tip speed, and $G_0 = 0.195\ \mathrm{J \cdot m^{-2}}$ is used in the present study. The terminal velocity is determined by equating the energy release rate G obtained by FEM to the critical energy release rate G_c in Equation (4); a larger G for forward rolling then yields a larger terminal velocity v than that for backward rolling. Figure 4b shows the predicted G-v curves for forward and backward rolling, which agree well with the experiments. It should be pointed out that $G_0 = 0.195\ \mathrm{J \cdot m^{-2}}$ used in the present study of discrete PDMS posts is smaller than that reported by Feng et al.[12] for a continuous PDMS film. This result is reasonable because the PDMS/glass energy release rate reported in the present experiments is averaged over the entire area, including the gaps between PDMS posts.

A shaking table test provides another way to visualize this behavior. Here, the roller stamp was placed on a flat, leveled glass substrate mounted on a motorized stage. As shown in

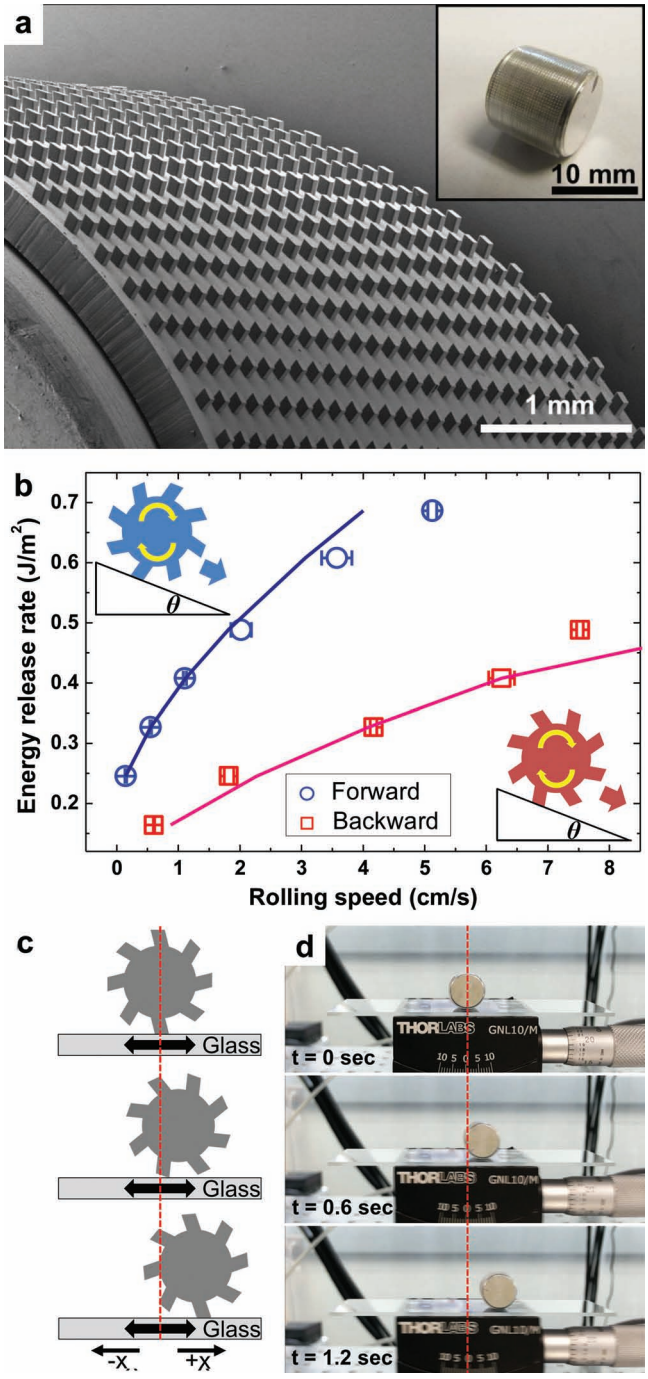

Figure 4. Demonstrations of rotation direction-dependent adhesion of an angled post roller. (a) SEM image of a cylinder surface wrapped by a flexible stamp with an array of angled posts. The inset shows a photograph of a stamp roller. (b) Energy release rate of an angled post roller as a function of rolling speed with two different orientations of the angled posts with respect to an inclined glass plate. Symbols and lines represent experimental and theoretical results, respectively. The insets in the upper left and lower right corners provide schematic representations for forward (high adhesion) and backward (low adhesion) rolling, respectively. (c) Schematic illustrations and (d) images of an angled post roller, moving in a preferred direction (+*x*) on a glass substrate, as a result of symmetric, oscillatory motion of the substrate.

Figure 4c, when the stage was accelerated along +*x* direction, the roller tended to roll in the opposite, -*x* direction, because of torque applied to the roller (counter clockwise). In this case, the angled post configuration lies against the torque direction, corresponding to the forward rolling direction where the high adhesion state impedes motion. For acceleration along the –*x* direction, the combination of the applied torque (clockwise) and the lower adhesion state of angled posts provided reduced resistance to rolling in the +*x* direction. The combined effect is that the roller moves in a preferential (+*x*) direction as a result of the symmetric oscillatory motion of stage along ±*x* direction (Figure 4d). The behaviors suggest that this kind of stamp is suitable for operation in a roller mode for transfer printing, where the retrieval process occurs on one side and the delivery on the other. Due to the symmetric geometry of a conventional, vertical post design, we do not expect any dependence of rolling speed on rolling direction or any preferential movement upon shaking.

In summary, adhesion switchability associated with angled features of relief in elastomer stamps for transfer printing offers new modes of high efficiency operation compared to previously reported cases. Theoretical analysis of the mechanics reveals the underlying elastic and viscoelastic physics, thereby providing routes for further optimization of the designs and the materials. Future work will focus on demonstrating these concepts in roll-to-roll transfer printing.

Experimental Section

Fabrication of elastomeric angled stamps: The fabrication involved soft lithographic procedures of casting and curing a prepolymer to PDMS (Sylgard 184, Dow Corning) against a photodefined collection of angled, square recesses (lateral dimensions of 100 μm × 100 μm; thickness ~ 100 μm) in a layer of epoxy (SU-8 50, Microchem). The patterning relied on ultraviolet (UV) exposure of a film of SU-8 on a silicon wafer coated with an antireflection layer (XHRiC-16, Brewer Science) and an adhesion promoter (OmniCoat, Microchem), mounted on a stage tilted to an angle of 34°. Developing away the unexposed regions of the SU-8, functionalizing the native oxide surface of the silicon with a fluorinated silane (tridecafluoro-1,1,2,2-tetrahydrooctyl-1-trichlorosilane, Gelest), casting a mixture of PDMS (Sylgard 184, Dow Corning; 5:1 ratio of prepolymer to curing agent) on top, thermally curing (70 °C for 1 h in convection oven), and peeling away the PDMS yielded an elastomeric angled stamp.

Transfer printing: Transfer printing followed the steps shown in Figure S3. In particular, an angled stamp mounted on a holder provided precise translational, rotational and vertical positional control relative to donor/receiver substrates. Automated stages controlled shear motion and retraction speeds.

Rolling and shaking tests: The roller consisted of an aluminum cylinder (9.5 mm of diameter, 9.5 mm of height and 1.915 g of mass) wrapped with a thin, flexible stamp that had an array of angled relief features (total 1820 angled reliefs in an array, area of an array of 8.2 mm × 19.3 mm, lateral dimensions of each relief of 100 μm × 100 μm with height of 100 μm, center to center distance between relief structures of 300 μm, angle of 17° relative to the normal to the backing layer surface). Placing such an object on an inclined glass plate led to rolling motion, driven by gravity. A ruler placed near the rolling path and a video camera allowed measurement of both the rolling distance and time. The terminal velocity corresponds to the constant speed reached by the roller, as determined from the video footage.

The shaking table test involved the same type of roller placed on a glass slide supported by manual tilting stage and an underlying

motorized stage. A customized LABVIEW interface controlled the stage to provide an oscillatory, or 'shaking', motion along one axis, with an acceleration of ± 2.54 m/sec^2 and a distance range of ± 2 mm. Adjusting the tilting stage allowed accurate leveling of the system.

Supporting Information

Supporting Information is available from the Wiley Online Library or from the author.

Acknowledgements

This material is based upon work supported by a National Security Science and Engineering Faculty Fellowship and the U.S. Department of Energy, Division of Materials Sciences under Award No. DEFG02–07ER46471, through the Frederick Seitz MRL and Center for Microanalysis of Materials at the University of Illinois at Urbana-Champaign. For the printing work, the authors also acknowledge the center for Nanoscale Chemical Electrical Mechanical Manufacturing Systems in University of Illinois, which is funded by the National Science Foundation under grant CMMI07-49028.

Received: December 30, 2011
Published online: March 19, 2012

[1] D. Chanda, K. Shigeta, S. Gupta, T. Cain, A. Carlson, A. Mihi, A. J. Baca, G. R. Bogart, P. Braun, J. A. Rogers, *Nat. Nanotechnol.* **2011**, *6*, 402.
[2] O. Fakhr, P. Altpeter, K. Karrai, P. Lugli, *Small* **2011**, *7*, 2533.
[3] S. W. Hong, F. Du, W. Lan, S. Kim, H.-S. Kim, J. A. Rogers, *Adv Mater* **2011**, *23*, 3821.
[4] T.-H. Kim, K.-S. Cho, E. K. Lee, S. J. Lee, J. Chae, J. W. Kim, D. H. Kim, J.-Y. Kwon, G. Amaratunga, S. Y. Lee, B. L. Choi, Y. Kuk, J. M. Kim, K. Kim, *Nat. Photonics* **2011**, *5*, 176.
[5] R.-H. Kim, D.-H. Kim, J. Xiao, B. H. Kim, S.-I. Park, B. Panilaitis, R. Ghaffari, J. Yao, M. Li, Z. Liu, V. Malyarchuk, D. G. Kim, A.-P. Le, R. G. Nuzzo, D. L. Kaplan, F. G. Omenetto, Y. Huang, Z. Kang, J. A. Rogers, *Nat. Mater.* **2010**, *9*, 929.
[6] H. Ko, K. Takei, R. Kapadia, S. Chuang, H. Fang, P. W. Leu, K. Ganapathi, E. Plis, H. S. Kim, S.-Y. Chen, M. Madsen, A. C. Ford, Y.-L. Chueh, S. Krishna, S. Salahuddin, A. Javey, *Nature* **2010**, *468*, 286.
[7] C. E. Packard, A. Murarka, E. W. Lam, M. A. Schmidt, V. Bulovic, *Adv Mater* **2010**, *22*, 1840.
[8] J. Yoon, S. Jo, I. S. Chun, I. Jung, H.-S. Kim, M. Meitl, E. Menard, X. Li, J. J. Coleman, U. Paik, J. A. Rogers, *Nature* **2010**, *465*, 329.
[9] S. Kim, J. Wu, A. Carlson, S. H. Jin, A. Kovalsky, P. Glass, Z. Liu, N. Ahmed, S. L. Elgan, W. Chen, P. M. Ferreira, M. Sitti, Y. Huang, J. A. Rogers, *Proc. Natl. Acad. Sci. USA* **2010**, *107*, 17095.
[10] Z. Fan, J. C. Ho, T. Takahashi, R. Yerushalmi, K. Takei, A. C. Ford, Y.-L. Chueh, A. Javey, *Adv. Mater.* **2009**, *21*, 3730.
[11] M. A. Meitl, Z. T. Zhu, V. Kumar, K. J. Lee, X. Feng, Y. Y. Huang, I. Adesida, R. G. Nuzzo, J. A. Rogers, *Nat. Mater.* **2006**, *5*, 33.
[12] X. Feng, M. A. Meitl, A. M. Bowen, Y. Huang, R. G. Nuzzo, J. A. Rogers, *Langmuir* **2007**, *23*, 12555.
[13] K. Autumn, Y. A. Liang, S. T. Hsieh, W. Zesch, W. P. Chan, T. W. Kenny, R. Fearing, R. J. Full, *Nature* **2000**, *405*, 681.
[14] S. Gorb, *Proc. R. Soc. B-Biol. Sci.* **1998**, *265*, 747.
[15] T. Eisner, D. J. Aneshansley, *Proc. Natl. Acad. Sci. USA* **2000**, *97*, 6568.
[16] W. Federle, *Integr. Comp. Biol.* **2002**, *42*, 1100.
[17] K. Autumn, M. Sitti, Y. A. Liang, A. M. Peattie, W. R. Hansen, S. Sponberg, T. W. R. Kenny, J. N. Fearing, R. J. Israelachvili, *Proc. Natl. Acad. Sci. USA* **2002**, *99*, 12252.
[18] K. Autumn, A. Dittmore, D. Santos, M. Spenko, M. Cutkosky, *J. Exp. Biol.* **2006**, *209*, 3569.
[19] M. P. Murphy, B. Aksak, M. Sitti, *Small* **2009**, *5*, 170.
[20] B. Aksak, M. P. Murphy, M. Sitti, *Langmuir* **2007**, *23*, 3322.
[21] H. E. Jeong, J.-K. Lee, H. N. Kim, S. H. Moon, K. Y. Suh, *Proc. Natl. Acad. Sci. USA* **2009**, *106*, 5639.
[22] S. Kim, M. Spenko, S. Trujillo, B. Heyneman, D. Santos, M. R. Cutkosky, *IEEE Trans. Robot.* **2008**, *24*, 65.
[23] A. Carlson, H.-J. Kim-Lee, J. Wu, P. Elvikis, H. Cheng, A. Kovalsky, S. Elgan, Q. Yu, P. M. Ferreira, Y. Huang, K. T. Turner, J. A. Rogers, *Appl Phys Lett* **2011**, *98*, 264104.
[24] H. Tada, P. C. Paris, G. R. Irwin, *The Stress Analysis of Cracks Handbook*, New York **2000**.
[25] Y. Huang, W. Zhou, K. J. Hsia, E. Menard, J.-U. Park, J. R. Rogers, A. G. Alleyne, *Langmuir* **2005**, *21*, 17.